

Characterization of Structural Disorder in $\gamma\text{-Ga}_2\text{O}_3$

Helen. Y. Playford,^{†,§} Alex C. Hannon,[§] Matthew G. Tucker,[§] Daniel M. Dawson,^{||} Sharon E. Ashbrook,^{||} Reza J. Kastiban,[‡] Jeremy Sloan,[‡] and Richard I. Walton*,[†]

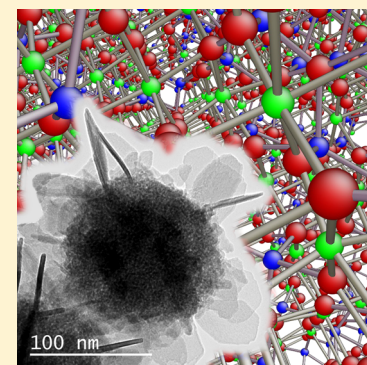
[†]Department of Chemistry and [‡]Department of Physics, University of Warwick, Coventry, CV4 7AL, United Kingdom

[§]ISIS Facility, Rutherford Appleton Laboratory, Didcot, OX11 0QX, United Kingdom

^{||}School of Chemistry, EaStCHEM and St Andrews Centre for Magnetic Resonance, St Andrews, KY16 9ST, United Kingdom

Supporting Information

ABSTRACT: Solvothermal oxidation of metallic gallium in monoethanolamine for 72 h at 240 °C yields a crystalline sample of $\gamma\text{-Ga}_2\text{O}_3$ (~30 nm crystallites). While Rietveld refinement (cubic spinel structure, $Fd\bar{3}m$; $a = 8.23760(9)$ Å) reveals that Ga occupies two pairs of octahedral and tetrahedral sites (ideal spinel and nonspinel), it provides no information about their local distribution, which cannot be statistical owing to the short Ga–Ga contacts produced if neighboring ideal spinel and nonspinel sites are simultaneously occupied. To create an atomistic model to reconcile this situation, a 6 × 6 × 6 supercell of the crystal structure is constructed and refined against neutron total scattering data using a reverse Monte Carlo (RMC) approach. This accounts well for the local as well as long-range structure and reveals significant local distortion in the octahedral sites that resembles the structure of thermodynamically stable $\beta\text{-Ga}_2\text{O}_3$. ^{71}Ga solid-state NMR results reveal a octahedral:tetrahedral Ga ratio that is consistent with the model obtained from RMC. Nanocrystalline samples of $\gamma\text{-Ga}_2\text{O}_3$ are produced by either a short solvothermal reaction (240 °C for 11 h in diethanolamine; ~15 nm crystallites) or by precipitation from an ethanolic solution of gallium nitrate (~5 nm crystallites). For these samples, the Bragg scattering profile is broadened by their smaller crystallite size, consistent with transmission electron microscopy results, and analysis of the relative Bragg peak intensities provides evidence that a greater proportion of tetrahedral versus octahedral sites are filled. In contrast, neutron total scattering shows the same average Ga–O distance with decreasing particle size, consistent with ^{71}Ga solid-state NMR results that indicate that all samples contain the same overall proportion of octahedral:tetrahedral Ga. It is postulated that increased occupation of tetrahedral sites within the smaller crystallites is balanced by an increased proportion of octahedral surface Ga sites, owing to termination by bound solvent or hydroxide.



INTRODUCTION

The structure of $\gamma\text{-Ga}_2\text{O}_3$ is recognized as being similar to that of $\gamma\text{-Al}_2\text{O}_3$, a cubic, cation-deficient spinel with partial occupancy of both tetrahedral and octahedral sites.¹ The relative proportion of occupied sites and their distribution, however, gives rise to inherent structural disorder that makes this analogy more complex. The catalytic chemistry of $\gamma\text{-Al}_2\text{O}_3$ has been widely investigated, and indeed its use as a catalyst support is commonplace.² The solid solution $\gamma\text{-Ga}_2\text{O}_3\text{-}\gamma\text{-Al}_2\text{O}_3$ has also been investigated for specific catalysis applications, and it is believed that preferential occupation of the tetrahedral sites by gallium leads to unique properties for the surface aluminum, such as in methane-selective catalytic reduction of NO,^{3–6} and in the dehydrogenation of propene.^{7–9} $\gamma\text{-Ga}_2\text{O}_3$ has itself been studied for various applications in catalysis and compared with other Ga_2O_3 polymorphs; for example, in the steam reforming of methanol¹⁰ and the photocatalytic degradation of volatile organics.^{11,12} Recently Lueangchaichaweng et al. have reported the use of gallium oxide nanorods, largely the γ polymorph, as highly effective catalysts for epoxidation reactions of alkenes.¹³ Interesting optical properties have also been a focus of recent attention for $\gamma\text{-Ga}_2\text{O}_3$; Chen et al. described the formation of

quantum dots with blue-green photoluminescence,¹⁴ which Wang et al. showed was particle-size controllable^{15–17} and could be enhanced by inducing defects under reductive conditions.¹⁸ The formation of mesoporous $\gamma\text{-Ga}_2\text{O}_3$ has been reported,^{19,20} and recently the growth of thin films of $\gamma\text{-Ga}_2\text{O}_3$ has been explored.²¹ It is also relevant to note that that various transition-metal-containing gallium oxides with spinel structures have recently been investigated and studied for their magnetic, optical, and photocatalytic properties.^{22–30}

Unlike the structures of alumina polymorphs, the structures of several of the gallia polymorphs have resisted characterization until our recent work that highlighted how structural disorder is common in the various forms of Ga_2O_3 .³¹ All samples of $\gamma\text{-Ga}_2\text{O}_3$ described in the literature have been produced by solution methods because thermal treatment readily leads to collapse to the thermodynamically stable $\beta\text{-Ga}_2\text{O}_3$.^{32–36} These synthesis routes tend to produce small particles, which then introduces further complications in

Received: April 6, 2014

Revised: June 25, 2014

Published: June 30, 2014

structural investigation because Bragg diffraction peaks are broadened and surface structure may become significant. Indeed, until our recent work, in which we performed Rietveld refinement of the structure against powder neutron diffraction data,³¹ only the cubic unit cell parameter of $\gamma\text{-Ga}_2\text{O}_3$ had been reported.¹ Our Rietveld analysis of this material revealed a defective spinel structure ($Fd\bar{3}m$; $a = 8.23760(9)$ Å) with gallium distributed over four sites: the expected tetrahedral 8 a and octahedral 16 d sites and additional tetrahedral 48 f and octahedral 16 c sites,³¹ similar to that found in $\gamma\text{-Al}_2\text{O}_3$ from single-crystal X-ray diffraction.³⁷ The refined octahedral:tetrahedral ratio is 1.35:1 for this crystalline $\gamma\text{-Ga}_2\text{O}_3$, compared to 1.70:1 for $\gamma\text{-Al}_2\text{O}_3$. The refined average structure does not, however, describe the distribution of gallium atoms because this cannot be completely random as physically implausible Ga–Ga distances (<2.4 Å) would result from the occupation of the 48 f and 16 c sites adjacent to the ideal spinel 8 a and 16 d sites. Furthermore, the local environment of gallium within the octahedral sites is likely to be asymmetrical if the structures of $\alpha\text{-Ga}_2\text{O}_3$ ³⁸ and $\beta\text{-Ga}_2\text{O}_3$ ³⁹ are considered, both of which have been refined from single crystal diffraction. These discrepancies between average and local structure were not resolved in our previous work, in which we used pair distribution function (PDF) analysis to refine the crystal structure; it proved impossible to fit the local structure of $\gamma\text{-Ga}_2\text{O}_3$ with the average model, though the medium-to-long-range structure was very well-described. In this paper we consider the structure of $\gamma\text{-Ga}_2\text{O}_3$ in detail; first by using a reverse Monte Carlo (RMC) refinement technique to obtain an atomistic model consistent with both local and average structure of a moderately crystalline sample, and then by examining two samples with smaller crystallite sizes, where we use neutron total scattering and solid-state NMR spectroscopy in conjunction with traditional diffraction analysis to develop a consistent picture of the structure of the material.

■ EXPERIMENTAL SECTION

Three samples of $\gamma\text{-Ga}_2\text{O}_3$ were prepared. The first (“crystalline”) was formed by the solvothermal oxidation of metallic gallium, based on the method of Kim et al.,³⁵ but optimized to give the most crystalline product at lower temperatures. Ga (0.3 g; Aldrich 99.99%) and monoethanolamine (5 mL; Aldrich ≥99.0%) were placed in a Teflon-lined stainless steel autoclave which was sealed and transferred to a preheated fan oven at 240 °C for 72 h. The solid product was dispersed into 10 mL of hot methanol, recovered by suction filtration, washed with further methanol, and dried at 70 °C overnight. The second sample (“nanocrystalline”) was prepared using a shorter time: 0.3 g of Ga (Aldrich 99.99%) and approximately 5 mL of diethanolamine (Aldrich ≥98.5%) were placed in a Teflon-lined stainless steel autoclave which was sealed and transferred to a preheated fan oven at 240 °C for 11 h. The reaction product, a fine white powder suspended in a viscous solvent, was dispersed into 15 mL of methanol, passed through a coarse filter to separate any pieces of unreacted gallium, and then isolated and washed with methanol via centrifugation before being dried at 70 °C overnight. The third sample was prepared using an aqueous route, similar to that of Areán et al.¹⁹ Gallium nitrate hydrate (3 g, Aldrich 99.9% metals basis) was dissolved in ethanol (50 mL), and concentrated aqueous ammonia, diluted 50% v/v with ethanol, was added to achieve a pH of 9.0. The resulting precipitate was

immediately filtered, washed with ethanol, and dried at 70 °C for 12 h before being calcined at 500 °C in air for 1 h.

For comparison, samples of $\alpha\text{-Ga}_2\text{O}_3$ and $\beta\text{-Ga}_2\text{O}_3$ were also prepared. $\alpha\text{-Ga}_2\text{O}_3$ was synthesized in two stages, using a procedure similar to those reported by Lavalle et al.⁴⁰ and Hou et al.¹¹ Gallium nitrate hydrate (3.0 g, Aldrich, 99.9% metals basis) was dissolved in distilled water (50 mL), and concentrated aqueous ammonia, diluted 50% v/v with distilled water, was added until no further precipitation was observed. The solution was left to stand overnight; then, a fine white precipitate was collected by vacuum filtration, washed with water and acetone, and dried at 70 °C overnight. This GaO(OH) product was heated at 500 °C for 4 h to yield phase-pure $\alpha\text{-Ga}_2\text{O}_3$.³⁸ A reference sample of $\beta\text{-Ga}_2\text{O}_3$ ³⁹ was obtained by heating gallium nitrate hydrate at 220 °C in air for 18 h, followed by regrinding and heating the product at 800 °C in air for 22 h.

Preliminary sample assessment was made using powder X-ray diffraction: patterns were recorded using a Siemens D5000 X-ray diffractometer operating with Cu K α radiation. Infrared spectra were recorded from the solid samples using a PerkinElmer Spectrum100 diamond attenuated total reflection–Fourier transform infrared (ATR-FTIR) spectrometer. Thermogravimetric analysis (TGA) was performed using a Mettler Toledo TGA/DSC1 instrument. Approximately 10 mg of powder were loaded into an alumina crucible; the sample was heated in air to 1000 °C at a rate of 10 °C min⁻¹. Transmission electron microscopy (TEM) measurements were made using a JEOL 2100 LaB₆ instrument, operating at 200 kV on specimens that were dispersed by ultrasound in ethanol and dropped onto 3 mm lacey carbon grids supplied by Agar.

Neutron total scattering experiments were performed using the instrument GEM^{41,42} at ISIS, the U.K. spallation neutron source. Each of the three samples of $\gamma\text{-Ga}_2\text{O}_3$ (~2 g) was separately loaded into vanadium cans with inner diameter 7.62 mm. Data were accumulated for approximately 5 h to ensure they were of good statistical quality. Data were also collected from an empty vanadium can, the empty instrument, and a vanadium rod for normalization purposes. Three banks of Bragg scattering data from GEM were analyzed simultaneously using the GSAS suite of software,⁴³ visualized with EXPGUI.⁴⁴ Total neutron scattering data analysis was performed by normalization of four banks of GEM data and merging them to produce the distinct scattering, $i(Q)$ ($Q_{\max} = 32$ Å⁻¹) using the GudrunN⁴⁵ and ATLAS⁴⁶ softwares. Fourier transformation of $i(Q)$, using a Lorch modification function, $M(Q)$,⁴⁷ to reduce the effect of termination ripples, yielded the differential correlation function $D(r)$, eq 1.

$$D(r) = \frac{2}{\pi} \int_0^{Q_{\max}} Q i(Q) M(Q) \sin rQ \, dQ \quad (1)$$

The function $D(r)$ is hereafter referred to as the pair distribution function (PDF). The program RMCProfile was used for reverse Monte Carlo modeling.⁴⁸ Data sets used for RMC refinements were the $i(Q)$ as mentioned above, and the total correlation function $T(r)$ (eq 3). Fitting was carried out to the $T(r)$ as the r weighting allows the medium range data to be fitted more accurately, whereas $G(r)$ is used for postrefinement visualization of the low- r region. For RMC the Fourier transform was carried out without the use of the Lorch function. The region of the correlation functions below $r = 1.7$ Å, which contained only nonphysical noise, was excluded from the RMC fit.

$$G(r) = \frac{D(r)}{4\pi r \rho_0} \quad (2)$$

$$T(r) = 4\pi r \rho_0 [G(r) + (\sum_{i=1}^n c_i \bar{b}_i)^2] \quad (3)$$

In these equations, ρ_0 is the number density and c_i and \bar{b}_i are the concentration and the neutron scattering length of the i th atom, respectively.

^{71}Ga solid-state NMR spectra were acquired at a magnetic field strength of 20.0 T. Samples were packed into 1.3 mm rotors and rotated at a MAS rate of 60 kHz. A spin echo was used to ensure undistorted lineshapes were acquired, with an echo duration, τ , of two rotor periods (33.33 μs) for α - and β - Ga_2O_3 and one rotor period (16.67 μs) for γ - Ga_2O_3 . Owing to the width of the lineshapes, high-power pulses (\sim 125 kHz radiofrequency nutation rate), of 1 and 2 μs for the first and second pulses, respectively, rather than central-transition selective pulses, were employed. For γ - Ga_2O_3 , the spectra were recorded with high-power pulses (\sim 200 kHz radiofrequency nutation rate) of 0.6 and 1.3 μs for the first and second pulses, respectively. While typically the first pulse must have a short flip angle to achieve (approximately) quantitative NMR spectra of quadrupolar nuclei, no significant variation in the relative intensity ratios of the tetrahedral, Ga(IV), and octahedral, Ga(VI), resonances was observed with increasing pulse length, whereas the overall signal was most intense with the pulse lengths used. Signal averaging was carried out for 2240 (α - Ga_2O_3), 7760 (β - Ga_2O_3), or 2048 (γ - Ga_2O_3) transients with a recycle interval of 3 s (α - and β - Ga_2O_3) or 1 s (γ - Ga_2O_3).

RESULTS

First we consider in detail the structure of the sample of “crystalline” γ - Ga_2O_3 prepared by the extended solvothermal oxidation of gallium metal. To obtain a model consistent with the distinct features of the average structure as well as the local scale disorder, we have used a reverse Monte Carlo (RMC) approach. Initially, a $5 \times 5 \times 5$ supercell of the crystal structure obtained from Rietveld refinement³¹ was created. Then, with each crystallographically distinct Ga site being treated separately, the correct proportion of “occupied” and “vacant” sites were created at random. This random distribution of atoms inevitably produces some unphysically short Ga–Ga correlations; therefore, the RMCProfile software was used to swap pairs of atoms and vacancies to reduce the number that violated a “minimum distance” constraint. During this process, no translational moves were allowed and no data were being fitted. Unfortunately, a point of stagnation, where no further swaps could be made, was always reached prior to all the unphysical correlations being removed. Therefore, an alternative strategy to build a starting configuration was sought. First, gallium atoms and vacancies were manually arranged in a $2 \times 2 \times 2$ supercell of the crystal structure such that there were no unphysical Ga–Ga distances. This configuration was then tripled to produce a $6 \times 6 \times 6$ supercell containing \sim 25 000 atoms for input into RMCProfile. The configuration thus produced contained artificial superstructure which caused extra peaks in the Bragg diffraction profile (Supporting Information); an atom-swapping procedure, driven by fitting to the Bragg profile, was therefore used to rerandomize the atomic arrangement. Because no translational moves were permitted,

only swaps that reduced the intensity of the spurious superstructure peaks improved the fit. In this manner, 20 different starting configurations were produced. For the full RMC refinements, each was duplicated 10 times, resulting in a total of 200 refined configurations per set. All refinements involved fitting to both the $i(Q)$ and the $T(r)$, with one set also including the Bragg profile as an additional data set. During refinement, the four crystallographic Ga sites were not segregated so as to avoid overly biasing the result toward the crystal structure. Instead, a bond valence sum constraint was used to keep the coordination environment of each Ga physically reasonable. A distance window constraint requiring atom pairs to remain within a window specified by an appropriate minimum and maximum distance was also used. Representative fits obtained after a run time of 72 h (after which time equilibrium was reached) can be seen in Figure 1. It should be noted that including or excluding the Bragg data had

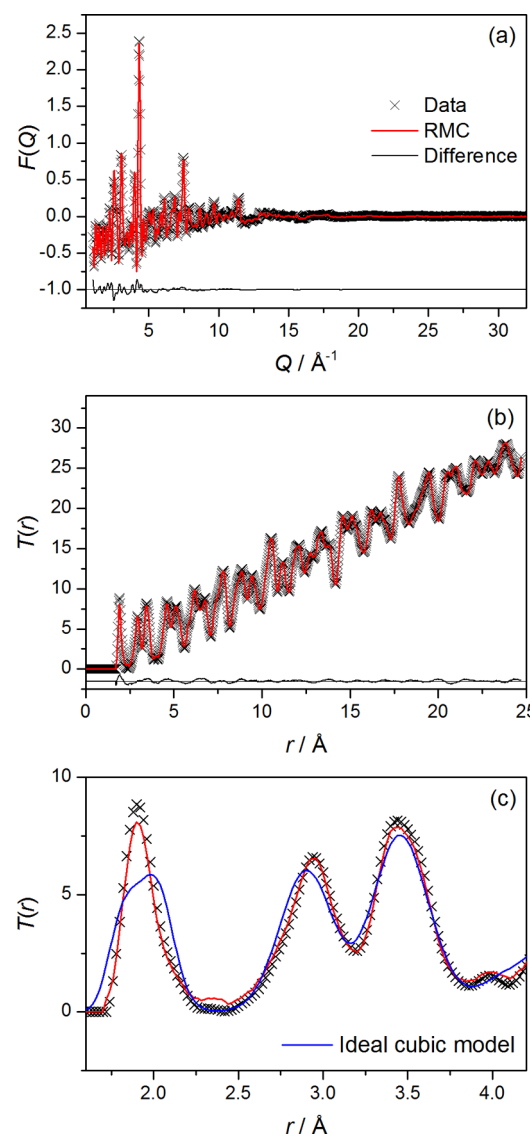


Figure 1. Representative final fits to neutron total scattering data from crystalline, solvothermal γ - Ga_2O_3 using RMC analysis: (a) fit to $F(Q)$, (b) fit to $T(r)$, and (c) expanded view of fit to $T(r)$ showing satisfactory resolution of local structure, compared with the $T(r)$ calculated from the ideal cubic structure.

no visible effect on the quality of the fits to $T(r)$ and $i(Q)$ (Supporting Information). As can be seen in Figure 1, the fits to the total scattering data in both real and reciprocal space are excellent. Of particular note is the good agreement in the low- r region of the $T(r)$, as this region is poorly described by the average structural model. To illustrate directly the relationship between the refined atomic configuration and the average starting structure, the supercell was folded back onto the original unit cell (Figure 2). The “clouds” of atoms in these illustrations represent the distribution of atoms around the average positions, and indeed for $\gamma\text{-Ga}_2\text{O}_3$ their centroids map directly back onto the coordinates of the crystallographic sites. Including the Bragg data in the refinements reduced the spread of the atom clouds, and indeed a comparison of calculated Bragg profiles (Supporting Information) shows that the model obtained is more appropriate for the average structure while, as we have already seen, being no less accurate for the local. All subsequent discussion therefore refers to the refinements that included Bragg data.

The Ga–O partial correlation functions for each different crystallographic site are shown in Figure 3. The pronounced asymmetry of the Ga_{16d} –O partial function shows that the $[\text{GaO}_6]$ octahedra are, on a local scale, distorted from cubic symmetry. Despite its small overall contribution to the total, the Ga_{16c} –O function is physically reasonable in shape and breadth (see Supporting Information), largely because of the application of the bond valence constraint. The summed Ga–Ga partial function compared with that calculated from the average structure is shown in Figure 4. There are no unphysically short correlations, and the peaks at 2.9 and 3.5 Å are slightly shifted and better defined in the RMC model with nonstatistical distribution of site occupation. Partial pair distribution functions for all possible combinations of pairs of unique Ga sites confirm that the main discrepancy when the Ga sites are statistically occupied is indeed in the unphysical short distance region, but also that some other discrepancies concerned with Ga–Ga distances are removed by allowing the local symmetry to relax (Supporting Information).

The mean Ga–O bond lengths for each site were calculated for each refined configuration and compared with the Rietveld averages (Table 1). The values are very similar and vary little from one refinement to the next. However, within each configuration the standard deviation in bond lengths for the octahedral sites is significantly larger than those for the tetrahedral, indicating a greater degree of disorder in the 6-coordinate sites. Distributions of O–Ga–O bond angles were calculated from 100 refined configurations and summed (Figure 5). For the ideal spinel sites, the distributions are symmetrical and centered upon the Rietveld values, but for the 48f tetrahedral site (which is rather distorted in the average, crystalline structure), the distribution has relaxed toward the ideal tetrahedral angle of 109.5°.

The polyhedral units in the refined configurations were further analyzed and categorized in terms of number of bonds longer or shorter than average. Surprisingly, some trends in polyhedra “type” were observed. For the tetrahedral sites, the majority (~52%) were of the 2 + 2 type (i.e., having two shorter and two longer bonds). For the octahedral sites, the majority had all 6 bonds shorter than average (54%), which is not surprising considering the skewness of the bond length distribution. The next most common type was found to be 3 + 3 type (38%), which is a significant observation given that the crystal structures of both $\alpha\text{-Ga}_2\text{O}_3$ and $\beta\text{-Ga}_2\text{O}_3$ contain

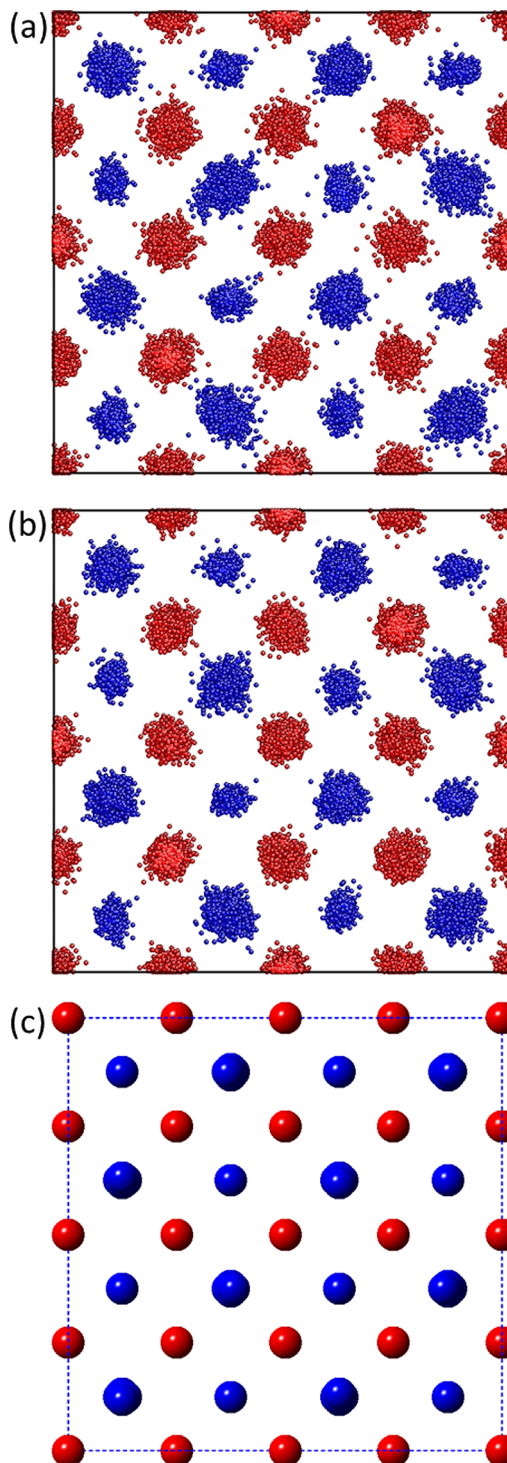


Figure 2. Group of 10 RMC refined configurations collapsed back onto the original unit cell, for the refinements without Bragg data (a) and with Bragg data (b). A projection of the crystal structure is shown in (c) for comparison. Red spheres are Ga atoms on octahedral sites, blue are Ga on tetrahedral sites. Oxygen atoms not shown.

$[\text{GaO}_6]$ sites of this type exclusively. RMC analysis therefore provides direct evidence for the similarity in local structure between metastable cubic $\gamma\text{-Ga}_2\text{O}_3$ and the thermodynamically stable monoclinic $\beta\text{-Ga}_2\text{O}_3$.

Having obtained a detailed structural model for the crystalline $\gamma\text{-Ga}_2\text{O}_3$ sample, we now consider the two materials prepared as smaller crystallites. Figure 6 shows TEM images of

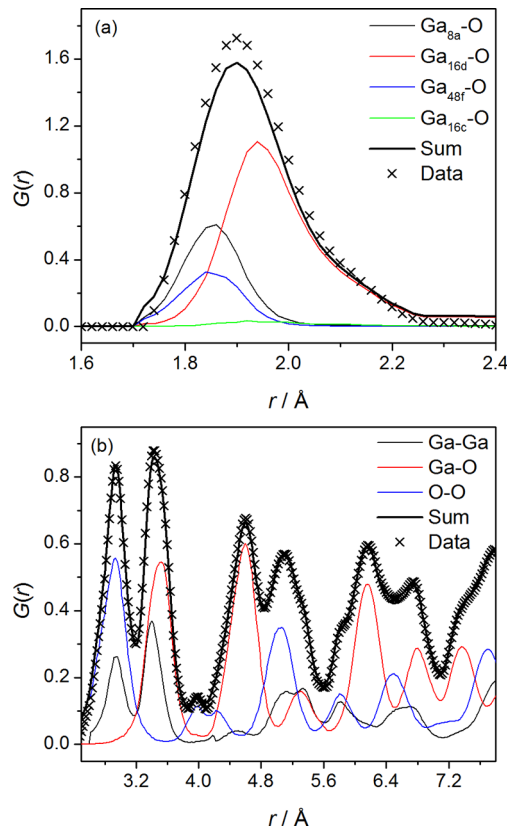


Figure 3. Partial PDFs of crystalline, solvothermal $\gamma\text{-Ga}_2\text{O}_3$. Measured data are points, and the lines are those simulated from a set of 10 refined RMC configurations. The Ga–O correlations for each crystallographic site are shown in (a) while, for clarity, the sum of these is shown in (b).

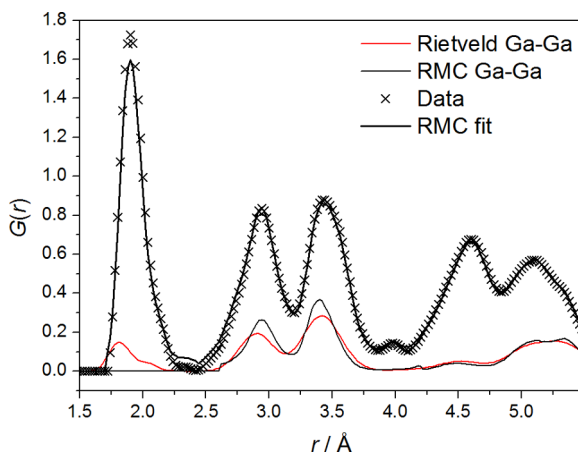


Figure 4. Comparison of Ga–Ga partials from Rietveld and RMC structural models. The unphysically short correlations in the average structure are clearly visible at $r < 2.0 \text{ \AA}$.

three samples. The most crystalline sample (Figure 6b) has a morphology that resembles that reported by Kim et al., who used the same synthesis method,¹⁸ and high-magnification images (Figure 6c) show individual particles to be made of agglomerates of platelike primary crystallites, typically of ~ 30 nm in maximum dimension. The “nanocrystalline” sample, prepared using a short solvothermal reaction, also is formed from the same platelike crystallites (Figure 6f), but the agglomerates are smaller (10–15 nm in dimension) and less

Table 1. Comparison of Mean Bond Lengths Obtained from RMC Refinements with Those from Rietveld Analysis for Crystalline $\gamma\text{-Ga}_2\text{O}_3$

	RMC bond length (\AA)	Rietveld bond length (\AA)	difference (%)
Ga 8a	1.8705(3)	1.85789(1)	0.69
Ga 16d	2.0064(2)	2.01736(2)	-0.55
Ga 48f	1.8553(3)	1.78738(1)	3.80
Ga 16c	2.015(1)	2.10323(2)	-4.18

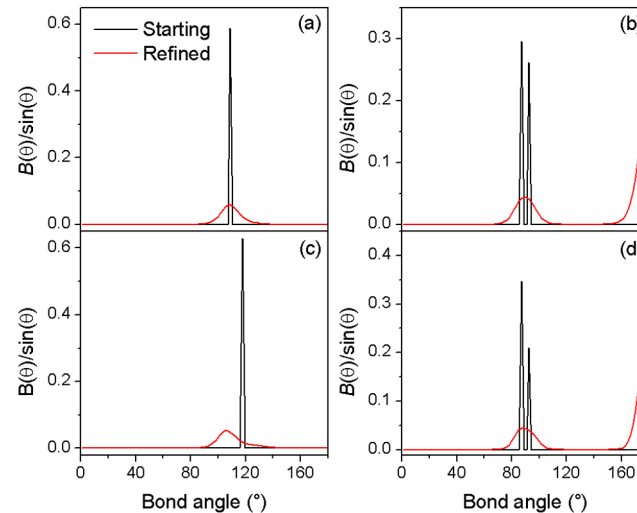


Figure 5. Comparison of O–Ga–O bond angles in the average structural model with the distributions of bond angles in the RMC configurations. $B(\theta)$ is the bond angle distribution function and the division by $\sin \theta$ accounts for the geometric factor when calculating bond angles. Distributions were calculated from 100 refined configurations and summed. Plots are for (a) 8a, (b) 16d, (c) 48f, and (d) 16c sites.

rough compared to those of the more crystalline sample (Figure 6e). The “disordered” sample, prepared from ethanolic solution, shows smaller particles (Figure 6h) and apparently also formed from platelike, primary crystallites, as the other two samples (Figure 6i), despite the different synthesis method. Electron diffraction measured from the particles shows polycrystalline rings, which can be indexed using the expected face-centered cubic unit cell (Figure 6a,d,g). Figure 7 shows neutron Bragg scattering of the three samples. Shorter solvothermal oxidation reactions yield a sample with a broadened diffraction profile (Figure 7b), consistent with the smaller crystallite size seen by TEM, but all Bragg peaks can clearly still be resolved. In contrast, the sample prepared by the aqueous precipitation method shows a considerably more broadened profile (Figure 7c) with the effect of small crystallite size much more apparent. Scherrer analysis of the diffraction profiles gave average crystallite sizes of 30, 15, and 5 nm for the “crystalline”, “nanocrystalline”, and “disordered” samples, respectively. A closer inspection of the Bragg scattering shows systematic changes in relative peak intensities in addition to the broadening of the profile (Figure 7d). Rietveld analysis of the nanocrystalline sample (Figures 7e,f) using the model for the crystalline sample as a starting point reveals that the lattice parameter is slightly smaller ($a = 8.2240(2) \text{ \AA}$, cf. $a = 8.23760(9) \text{ \AA}$ for the crystalline sample) and, more obviously, that the site occupancies are different (Table 2). The total ratio of octahedral to tetrahedral gallium is 1.14:1 for this material

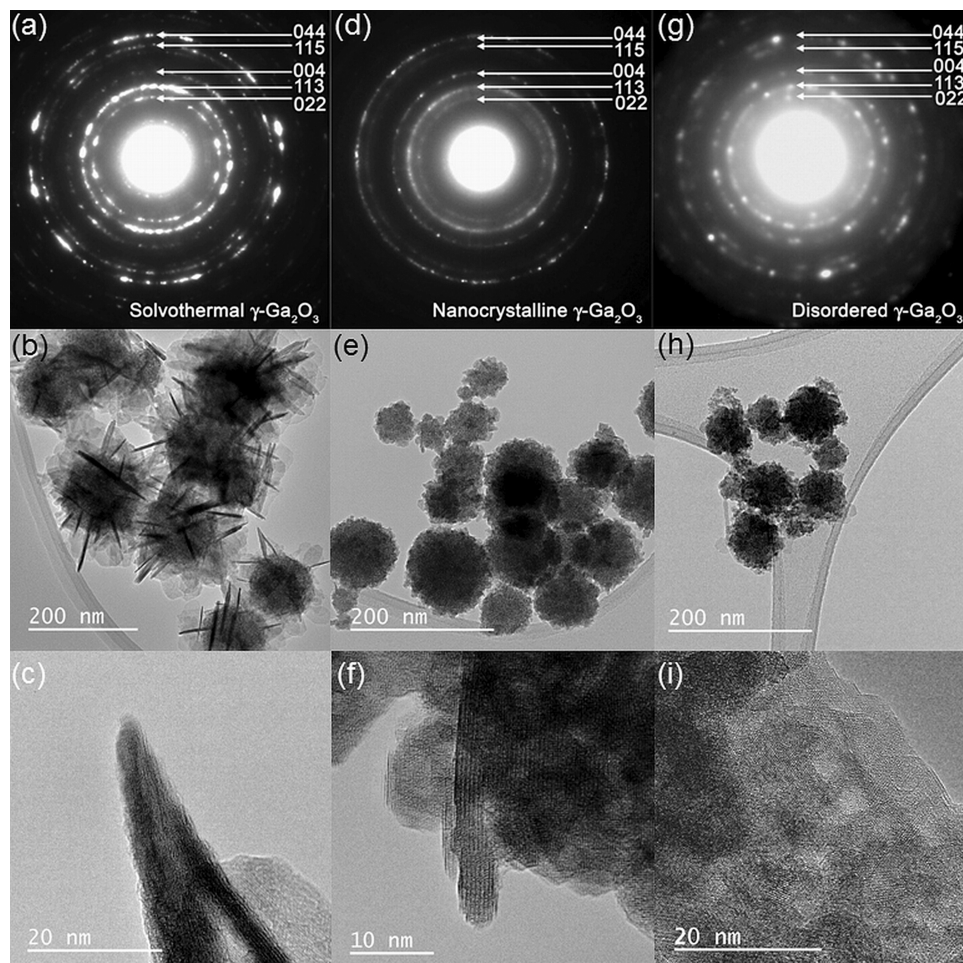


Figure 6. TEM of $\gamma\text{-Ga}_2\text{O}_3$ samples. Top row is electron diffraction indexed using the F-cubic unit cell seen by neutron diffraction, and middle and bottom rows are images at two magnifications from (a–c) crystalline $\gamma\text{-Ga}_2\text{O}_3$, (d–f) nanocrystalline $\gamma\text{-Ga}_2\text{O}_3$, and (g–i) disordered $\gamma\text{-Ga}_2\text{O}_3$.

(cf. 1.35:1 for the more crystalline sample), showing a greater number of tetrahedral sites are occupied and that the number of nonstandard spinel sites has increased: the ratio of spinel to nonspinel sites is 1.94:1, compared to 5:1 in crystalline $\gamma\text{-Ga}_2\text{O}_3$. Any attempt made to fit the diffraction profile without changing the site occupancies from the original crystal structure, and instead adding additional parameters like anisotropic thermal displacements, was unsuccessful.

The diffraction profile from the disordered sample made via precipitation proved impossible to fit meaningfully using Rietveld analysis, and the high background of the data may be due to incoherent scattering from a hydrogeneous contaminant material, such as surface-bound solvent. Furthermore, the apparent shift in the position of the (222) Bragg peak cannot be accounted for by the $\gamma\text{-Ga}_2\text{O}_3$ phase and may be caused by overlap with a broadened peak from a poorly crystalline impurity. Nevertheless, using the idea of an increase in tetrahedral relative to octahedral site occupancy with decreasing crystallite size (as seen for the previous sample) the Bragg peak intensities of the neutron diffraction pattern can be well-matched using a modified spinel structure with an octahedral:tetrahedral ratio of 0.82:1 and a spinel:non-spinel ratio of 0.51:1, which suggests that the trend seen going from crystalline to nanocrystalline solvothermal $\gamma\text{-Ga}_2\text{O}_3$ (i.e., an increase in the amount of tetrahedral gallium and increased occupancy of nonspinel sites) continues as the particle size

further decreases in the precipitated sample; this model is summarized in Table 3 and shown in Figure 8 where the simulated scattering function is compared with the observed.

The pair distribution functions of the nanocrystalline and disordered samples of $\gamma\text{-Ga}_2\text{O}_3$ show clear evidence of decreasing particle size, with an obvious dampening with increasing radial distance (Figure 9a). In the case of the nanocrystalline, solvothermal sample, the low- r region exhibits a strong peak at $\sim 1.5 \text{ \AA}$ that can be assigned to C–C or C=N bonds from residual solvent molecules (expected at 1.51 and 1.47 \AA , respectively) (Figure 9b); this is confirmed by IR spectroscopy and thermogravimetric analysis (Supporting Information), and we suggest that this is surface-bound solvent. The sample from ethanolic precipitation shows a hydrogeneous background in the neutron scattering, as noted above, and a larger proportion of surface water and/or hydroxide seen by TGA. The presence of secondary phases, which may in fact simply be surface-bound species, in both of these materials precludes the use of RMC analysis to analyze fully their structures. Nevertheless, an important observation from the comparison of the PDFs from all three samples is that the average Ga–O distance is invariant (Figure 9b). It should be noted that the peak at $\sim 2 \text{ \AA}$ in the PDF is a combination of all close Ga–O distances and the shorter tetrahedral and longer octahedral distances cannot be resolved. The observation that the average Ga–O coordination is unchanged on reducing

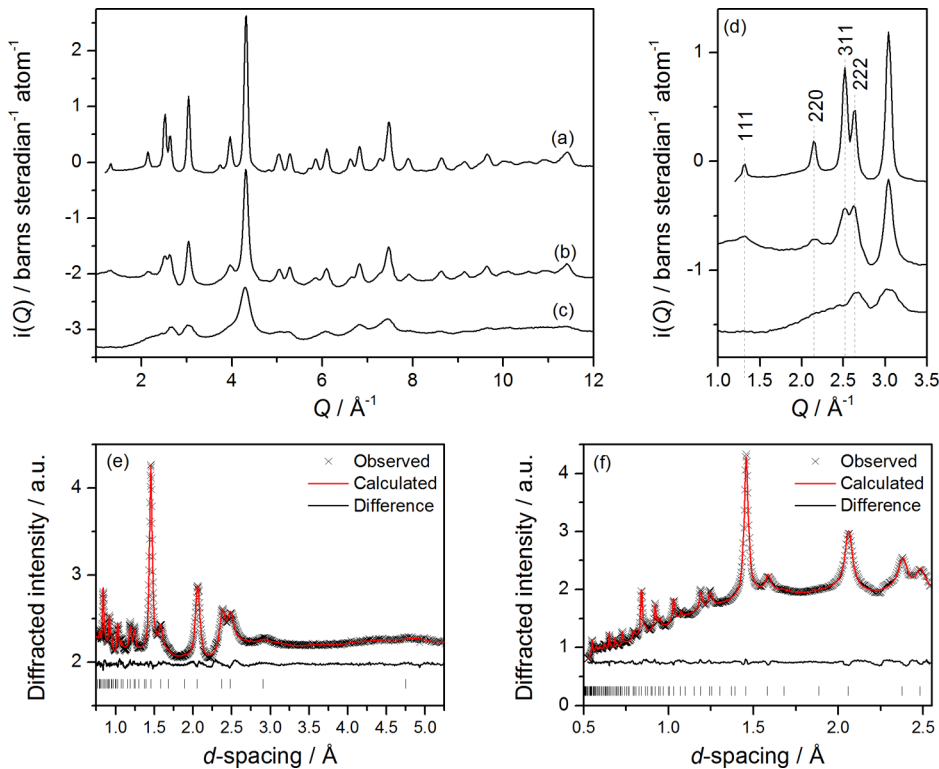


Figure 7. Neutron Bragg scattering for the three samples of γ -Ga₂O₃: (a) crystalline solvothermal sample, (b) nanocrystalline solvothermal sample, and (c) poorly crystalline precipitated sample. Panel d shows an expanded region highlighting changes in relative Bragg peak intensity, while (e) and (f) show a Rietveld fit of the profile for the nanocrystalline solvothermal sample for two banks of GEM data.

Table 2. Crystal Parameters from Nanocrystalline, Solvothermal γ -Ga₂O₃^a

atom	Wyckoff site	x	y	z	U_{iso} (\AA^2)	occupancy
Ga1	8a	0.125	0.125	0.125	0.0129(2)	0.54(2) [0.741(8)]
Ga2	16d	0.5	0.5	0.5	0.0129(2)	0.610(7) [0.741(3)]
Ga3	48f	0.348(1) [0.368(2)]	0.125	0.125	0.0129(2)	0.118(3) [0.066(1)]
Ga4	16c	0	0	0	0.0129(2)	0.100(6) [0.024(1)]
O	32e	0.251(3) [0.2552(1)]	0.251(3) [0.2552(1)]	0.251(3) [0.2552(1)]	0.0135(1)	1

^aSpace group $Fd\bar{3}m$; $a = 8.2240(2)$ \AA . $R_p = 0.66\%$; $wR_p = 0.92\%$. The italic values in square brackets are those for the crystalline, solvothermal material.³¹

Table 3. Modified Spinel Model Used to Describe Disordered γ -Ga₂O₃ Made by the Ethanolic Precipitation Method

atom	$Fd\bar{3}m$ site	x	y	z	occupancy
Ga1	8a	1/8	1/8	1/8	0.3
Ga2	8b	3/8	3/8	3/8	0.3
Ga3	16d	1/2	1/2	1/2	0.3
Ga4	16c	0	0	0	0.3
Ga5	48f	0.3679	1/8	1/8	0.1445
O	32e	0.2552	0.2552	0.2552	1

particle size is apparently inconsistent with the analysis of the Bragg scattering but in fact highlights the different views of the sample obtained from the different techniques. If the entirety of a sample volume is crystalline, then both Bragg diffraction and total scattering analyses should obtain the same fundamental structural parameters, such as average coordination number. If, however, a significant region of the sample is not crystalline, such as for small particles for which the surface becomes more significant, this is no longer the case. The Ga–O coordination observed in the PDF includes all Ga–O pairs in the sample,

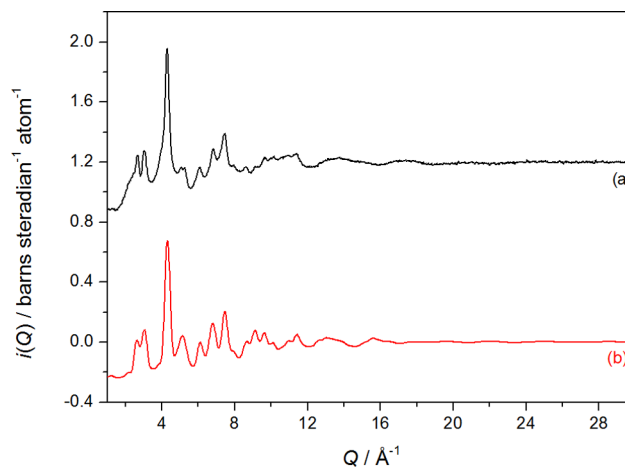


Figure 8. A comparison of the neutron $i(Q)$ from (a) disordered γ -Ga₂O₃ with (b) the $i(Q)$ simulated for the modified spinel model, adjusted for small particle size using a Mason factor.

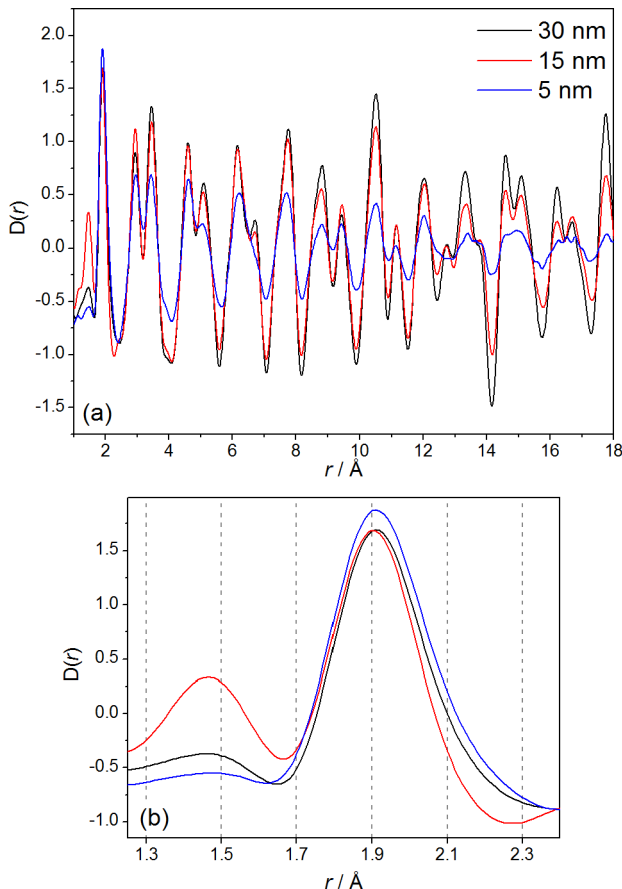


Figure 9. PDFs of the three $\gamma\text{-Ga}_2\text{O}_3$ materials: (a) the effect of decreasing particle size on the damping of the function and (b) the low- r region showing the contaminant C–C/C–N peak at $\sim 1.5 \text{\AA}$ in the $\sim 15 \text{ nm}$ solvothermal sample and the invariant Ga–O interatomic distance.

including those in disordered regions, such as the crystallite surfaces.

The ^{71}Ga NMR spectra of the three samples of $\gamma\text{-Ga}_2\text{O}_3$, shown in Figure 10, provide clear evidence of the disordered nature of the material, as all resonances observed display significant additional broadening (rather than the characteristic second-order quadrupolar lineshapes observed for the more ordered α - and β - polymorphs of Ga_2O_3 , shown in panels d and e of Figure 10, respectively), with asymmetric upfield “tails” indicative of a distribution of quadrupolar and chemical shift parameters. Indeed, even with the high B_0 field strength (20.0 T) and rapid MAS (60 kHz) used for this work, the isotropic tetrahedral and octahedral resonances remain slightly overlapped, although they are well-separated from the first spinning sidebands. It is interesting to note that although O’Dell et al. observed an increase in the disorder-related line broadening with decreasing particle size (down to $\sim 20 \text{ nm}$) for $\beta\text{-Ga}_2\text{O}_3$,⁴⁸ no such trend was observed here, most likely owing to the smaller particle size regime investigated and the inherently more disordered nature of $\gamma\text{-Ga}_2\text{O}_3$. The extent of the overlap of the resonances means that it was not possible to observe the distinct types of tetrahedral and octahedral Ga directly in the MAS spectra. However, from spectra recorded using short flip angles, ensuring that (approximate) quantification of the overall tetrahedral:octahedral ratio was possible, values of 1:1.8, 1:1.8, and 1:2.1 were obtained for the crystalline, nanocrystalline, and

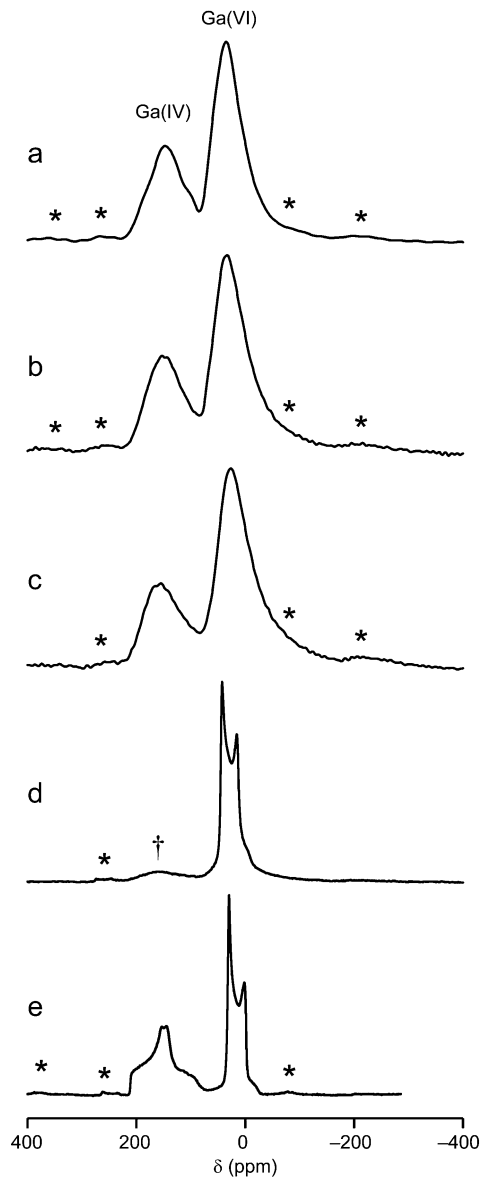


Figure 10. 1D ^{71}Ga (20.0 T, 60 kHz MAS) NMR spectra of (a) crystalline $\gamma\text{-Ga}_2\text{O}_3$, (b) nanocrystalline $\gamma\text{-Ga}_2\text{O}_3$, (c) disordered $\gamma\text{-Ga}_2\text{O}_3$, (d) $\alpha\text{-Ga}_2\text{O}_3$, and (e) $\beta\text{-Ga}_2\text{O}_3$. Asterisks denote spinning sidebands and, in panel d, \dagger denotes a Ga tetrahedral resonance assigned to surface reconstruction. Ga(IV) and Ga(VI) denote tetrahedral and octahedral gallium, respectively.

disordered samples of $\gamma\text{-Ga}_2\text{O}_3$, respectively. This result is consistent with the PDF analysis, which showed that the average Ga coordination environment does not change significantly between the three different particle sizes.

DISCUSSION

Our RMC analysis of $\gamma\text{-Ga}_2\text{O}_3$ reveals structural complexity in an apparently simple material, including pronounced local-scale deviation from the cubic average structure, and provides detailed information about the distribution of bond lengths and angles. This information is lacking from a crystallographic analysis alone. The structural model obtained using RMC is consistent with results from ^{71}Ga NMR which show heavily broadened resonances that can be assigned to mixtures of more than one type of both octahedral and tetrahedral Ga sites of

nonideal local symmetry. The effect of decreasing particle size apparently reduces the proportion of octahedral Ga sites compared to tetrahedral sites within the crystalline volume of the particles, as evidenced by Bragg scattering, but this must be compensated for by an increase in octahedral gallium because both the pair distribution functions and solid-state NMR results show an invariant octahedral:tetrahedral gallium ratio. A likely explanation is that an increased number of surface Ga sites is present for the sample of smaller particle size, and these have a different environment than the bulk. The surface chemistry of $\gamma\text{-Ga}_2\text{O}_3$ has received some consideration previously, owing to its relevance in catalysis applications, but our work is the first to examine structure directly using diffraction methods. In a series of papers by Areán and co-workers, a similarity between the surface chemistry of $\gamma\text{-Ga}_2\text{O}_3$ and $\alpha\text{-Ga}_2\text{O}_3$ was noted,⁴⁰ and by using IR spectroscopy with probe molecules such as CO and pyridine, they showed the presence of strong Lewis acid sites.^{50–52} Similar effects were seen for $\gamma\text{-Ga}_2\text{O}_3-\gamma\text{-Al}_2\text{O}_3$ solid.⁵³ The consensus was reached from these IR studies that coordinatively unsaturated, tetrahedral gallium sites at the surface were responsible for the strong binding of Lewis bases, including for $\alpha\text{-Ga}_2\text{O}_3$ whose bulk crystal structure contains only octahedral gallium. It is important to note that in these IR experiments the samples were heated for several hours under dynamic vacuum (typically 673 K, 10^{-4} Torr); thus, any pre-existing, surface-bound solvent or hydroxide will undoubtedly have been removed to “activate” the surface. For our materials, studied in an “as-made” state, from solution synthesis, the surface will have associated solvent, water, or hydroxide and so is most likely to be terminated as octahedral gallium, consistent with the picture we see by considering the results of all techniques applied.

CONCLUSIONS

Structural investigation of an apparently simple binary oxide has been made possible using several advanced structural probes, both diffraction-based and spectroscopic, which in combination provide a model for the nonstatistical occupation of partially filled metal sites and the balance of bulk versus surface metal sites. While Rietveld refinement shows that in $\gamma\text{-Ga}_2\text{O}_3$ the Ga occupies two pairs of octahedral and tetrahedral sites (ideal spinel and nonspinel), it provides no information about their local distribution, which cannot be statistical owing to the short Ga–Ga contacts produced if simultaneous occupation of neighboring ideal spinel and nonspinel sites occurs. Thus, refinement against neutron total scattering data using a reverse Monte Carlo (RMC) approach was used to produce a model that accounts for the local and long-range structure, but this also reveals significant local distortion in the octahedral sites that resembles the structure of thermodynamically stable polymorph of the same composition, $\beta\text{-Ga}_2\text{O}_3$. For nanocrystalline samples of the same material, analysis of the relative Bragg peak intensities reveals evidence for a greater proportion of tetrahedral versus octahedral sites. In contrast, neutron total scattering shows an invariant average Ga–O distance with particle size, itself consistent with ^{71}Ga solid-state NMR results that indicate that all samples contain the same overall proportion of octahedral:tetrahedral Ga. It is therefore proposed that increased occupation of tetrahedral sites within the smaller crystallites is matched by an increased proportion of octahedral surface Ga sites, most likely due to termination by bound solvent or hydroxide. This new insight into the inherent disorder of the structure and how it is affected by crystallite size

provides new information to further understand the Ga_2O_3 system, which is of importance given the recent interest in the catalytic and electronic properties of gallium oxides.

ASSOCIATED CONTENT

S Supporting Information

Further details of reverse Monte Carlo analysis of crystalline $\gamma\text{-Ga}_2\text{O}_3$ and general characterization data from all samples (TGA-DSC, IR, and TEM). This material is available free of charge via the Internet at <http://pubs.acs.org>.

AUTHOR INFORMATION

Corresponding Author

*E-mail: r.i.walton@warwick.ac.uk. Tel.: +44 (0)2476523241.

Notes

The authors declare no competing financial interest.

ACKNOWLEDGMENTS

We are grateful to the STFC for provision of beam time at ISIS and for part-funding a studentship for H.Y.P. through its Centre for Materials Physics and Chemistry (Grant CMPC08104). H.Y.P. also thanks the EPSRC for providing a Postdoctoral Prize Award (Grant EP/P50578X/1). We thank Mr. Luke Daniels for measuring the TGA data and Dr. Martin Mitchell for recording the ^{71}Ga NMR spectra of α - and $\beta\text{-Ga}_2\text{O}_3$. Some of the equipment used in materials characterization at the University of Warwick was obtained through the Science City Advanced Materials project “Creating and Characterizing Next Generation Advanced Materials” with support from Advantage West Midlands (AWM) and part funded by the European Regional Development Fund (ERDF). The UK 850 MHz solid-state NMR Facility used in this research was funded by EPSRC and BBSRC, as well as the University of Warwick. Computing resources were provided by STFC’s e-Science facility.

REFERENCES

- (1) Zinkevich, M.; Morales, F. M.; Nitsche, H.; Ahrens, M.; Ruhle, M.; Aldinger, F. Microstructural and Thermodynamic Study of $\gamma\text{-Ga}_2\text{O}_3$. *Z. Metallkd.* **2004**, *95*, 756–762.
- (2) Trueba, M.; Trasatti, S. P. γ -Alumina as a Support for Catalysts: A Review of Fundamental Aspects. *Eur. J. Inorg. Chem.* **2005**, 3393–3403.
- (3) Shimizu, K.; Takamatsu, M.; Nishi, K.; Yoshida, H.; Satsuma, A.; Tanaka, T.; Yoshida, S.; Hattori, T. Alumina-Supported Gallium Oxide Catalysts for NO Selective Reduction: Influence of the Local Structure of Surface Gallium Oxide Species on the Catalytic Activity. *J. Phys. Chem. B* **1999**, *103*, 1542–1549.
- (4) Nakatani, T.; Watanabe, T.; Takahashi, M.; Miyahara, Y.; Deguchi, H.; Iwamoto, S.; Kanai, H.; Inoue, M. Characterization of $\gamma\text{-Ga}_2\text{O}_3-\text{Al}_2\text{O}_3$ Prepared by Solvothermal Method and Its Performance for Methane-SCR of NO. *J. Phys. Chem. A* **2009**, *113*, 7021–7029.
- (5) Watanabe, T.; Miki, Y.; Masuda, T.; Kanai, H.; Hosokawa, S.; Wada, K.; Inoue, M. Performance of $\gamma\text{-Ga}_2\text{O}_3-\text{Al}_2\text{O}_3$ Solid Solutions Prepared by Spray Pyrolysis for CH_4 -SCR of NO. *Appl. Catal., A* **2011**, *396*, 140–147.
- (6) Watanabe, T.; Miki, Y.; Miyahara, Y.; Masuda, T.; Deguchi, H.; Kanai, H.; Hosokawa, S.; Wada, K.; Inoue, M. Enhancement of the Activities of $\gamma\text{-Ga}_2\text{O}_3-\text{Al}_2\text{O}_3$ Catalysts for Methane-SCR of NO by Treatment with NH_3 . *Catal. Lett.* **2011**, *141*, 1338–1344.
- (7) Zheng, B.; Hua, W. M.; Yue, Y. H.; Gao, Z. Dehydrogenation of Propane to Propene over Different Polymorphs of Gallium Oxide. *J. Catal.* **2005**, *232*, 143–151.
- (8) Xu, B. J.; Zheng, B.; Hua, W. M.; Yue, Y. H.; Gao, Z. Support Effect in Dehydrogenation of Propane in the Presence of CO_2 over Supported Gallium Oxide Catalysts. *J. Catal.* **2006**, *239*, 470–477.

- (9) Chen, M.; Xu, J.; Su, F. Z.; Liu, Y. M.; Cao, Y.; He, H. Y.; Fan, K. N. Dehydrogenation of Propane over Spinel-Type Gallia-Alumina Solid Solution Catalysts. *J. Catal.* **2008**, *256*, 293–300.
- (10) Collins, S. E.; Briand, L. E.; Gambaro, L. A.; Baltanas, M. A.; Bonivardi, A. L. Adsorption and Decomposition of Methanol on Gallium Oxide Polymorphs. *J. Phys. Chem. C* **2008**, *112*, 14988–15000.
- (11) Hou, Y. D.; Wu, L.; Wang, X. C.; Ding, Z. X.; Li, Z. H.; Fu, X. Z. Photocatalytic Performance of α -, β -, and γ - Ga_2O_3 for the Destruction of Volatile Aromatic Pollutants in Air. *J. Catal.* **2007**, *250*, 12–18.
- (12) Seshadri, H.; Cheralathan, M.; Sinha, P. K. Photocatalytic Performance of Combustion-Synthesized β and γ - Ga_2O_3 in the Degradation of 1,4-Dioxane in Aqueous Solution. *Res. Chem. Intermed.* **2013**, *39*, 991–1001.
- (13) Lueangchaichaweng, W.; Brooks, N. R.; Fiorilli, S.; Gobechiya, E.; Lin, K.; Li, L.; Parres-Eslapez, S.; Javon, E.; Bals, S.; Van Tendeloo, G.; et al. Gallium Oxide Nanorods: Novel, Template-Free Synthesis and High Catalytic Activity in Epoxidation Reactions. *Angew. Chem., Int. Ed.* **2014**, *53*, 1585–1589.
- (14) Chen, T.; Tang, K. B. γ - Ga_2O_3 Quantum Dots with Visible Blue-Green Light Emission Property. *Appl. Phys. Lett.* **2007**, *90*, 053104.
- (15) Wang, T.; Farvid, S. S.; Abulikemu, M.; Radovanovic, P. V. Size-Tunable Phosphorescence in Colloidal Metastable γ - Ga_2O_3 Nanocrystals. *J. Am. Chem. Soc.* **2010**, *132*, 9250–9252.
- (16) Wang, T.; Radovanovic, P. V. Size-Dependent Electron Transfer and Trapping in Strongly Luminescent Colloidal Gallium Oxide Nanocrystals. *J. Phys. Chem. C* **2011**, *115*, 18473–18478.
- (17) Hegde, M.; Wang, T.; Miskovic, Z. L.; Radovanovic, P. V. Origin of Size-Dependent Photoluminescence Decay Dynamics in Colloidal γ - Ga_2O_3 Nanocrystals. *Appl. Phys. Lett.* **2012**, *100*.
- (18) Wang, T.; Radovanovic, P. V. In Situ Enhancement of the Blue Photoluminescence of Colloidal Ga_2O_3 Nanocrystals by Promotion of Defect Formation in Reducing Conditions. *Chem. Commun. (Cambridge, U.K.)* **2011**, *47*, 7161–7163.
- (19) Areán, C. O.; Bellan, A. L.; Mentrut, M. P.; Delgado, M. R.; Palomino, G. T. Preparation and Characterization of Mesoporous γ - Ga_2O_3 . *Microporous Mesoporous Mater.* **2000**, *40*, 35–42.
- (20) Deshmame, C. A.; Jasinski, J. B.; Carreon, M. A. Microwave-Assisted Synthesis of Nanocrystalline Mesoporous Gallium Oxide. *Microporous Mesoporous Mater.* **2010**, *130*, 97–102.
- (21) Mitome, M.; Kohiki, S.; Nagai, T.; Kurashima, K.; Kimoto, K.; Bando, Y. A Rhombic Dodecahedral Honeycomb Structure with Cation Vacancy Ordering in a γ - Ga_2O_3 Crystal. *Cryst. Growth Des.* **2013**, *13*, 3577–3581.
- (22) Hayashi, H.; Huang, R.; Ikeno, H.; Oba, F.; Yoshioka, S.; Tanaka, I.; Sonoda, S. Room Temperature Ferromagnetism in Mn-Doped γ - Ga_2O_3 with Spinel Structure. *Appl. Phys. Lett.* **2006**, *89*, 181903.
- (23) Sakata, Y.; Matsuda, Y.; Nakagawa, T.; Yasunaga, R.; Immura, H.; Teramura, K. Remarkable Improvement of the Photocatalytic Activity of Ga_2O_3 Towards the Overall Splitting of H_2O . *ChemSusChem* **2011**, *4*, 181–184.
- (24) Yuan, Y. P.; Du, W. M.; Qian, X. F. $\text{Zn}_x\text{Ga}_2\text{O}_{3+x}$ ($0 \leq x \leq 1$) Solid Solution Nanocrystals: Tunable Composition and Optical Properties. *J. Mater. Chem.* **2012**, *22*, 653–659.
- (25) Conrad, F.; Bauer, M.; Sheptyakov, D.; Weyeneth, S.; Jaeger, D.; Hametner, K.; Car, P. E.; Patscheider, J.; Gunther, D.; Patzke, G. R. New Spinel Oxide Catalysts for Visible-Light-Driven Water Oxidation. *RSC Adv.* **2012**, *2*, 3076–3082.
- (26) Conrad, F.; Bauer, M.; Weyeneth, S.; Zhou, Y.; Hametner, K.; Gunther, D.; Patzke, G. R. Hierarchically Structured Copper Gallium Spinels through Microwave Hydrothermal Methods. *Solid State Sci.* **2013**, *24*, 125–132.
- (27) Duan, X. L.; Yu, F. P.; Wu, Y. C. Microstructure and Optical Properties of $\text{Co}_x\text{Zn}_{1-x}\text{Ga}_2\text{O}_4$ ($0 \leq x \leq 1$) Nanoparticles. *Eur. J. Inorg. Chem.* **2013**, 1287–1293.
- (28) Playford, H. Y.; Hannon, A. C.; Tucker, M. G.; Lees, M. R.; Walton, R. I. Total Neutron Scattering Investigation of the Structure of a Cobalt Gallium Oxide Spinel Prepared by Solvothermal Oxidation of Gallium Metal. *J. Phys.: Condens. Matter* **2013**, *25*, 454212.
- (29) Jia, C. Y.; Fan, W. L.; Yang, F.; Zhao, X.; Sun, H. G.; Li, P.; Liu, L. A Theoretical Study of Water Adsorption and Decomposition on Low-Index Spinel ZnGa_2O_4 Surfaces: Correlation between Surface Structure and Photocatalytic Properties. *Langmuir* **2013**, *29*, 7025–7037.
- (30) Xu, X. X.; Azad, A. K.; Irvine, J. T. S. Photocatalytic H_2 Generation from Spinels ZnFe_2O_4 , ZnFeGaO_4 and ZnGa_2O_4 . *Catal. Today* **2013**, *199*, 22–26.
- (31) Playford, H. Y.; Hannon, A. C.; Barney, E. R.; Walton, R. I. Structures of Uncharacterised Polymorphs of Gallium Oxide from Total Neutron Diffraction. *Chem.—Eur. J.* **2013**, *19*, 2803–2813.
- (32) Böhm, J. Über Galliumoxyd und -hydroxyd. *Angew. Chem.* **1940**, *53*, 131.
- (33) Roy, R.; Hill, V. G.; Osborn, E. F. Polymorphism of Ga_2O_3 and the System Ga_2O_3 – H_2O . *J. Am. Chem. Soc.* **1952**, *74*, 719–722.
- (34) Pohl, K. Hydrothermale Bildung von γ - Ga_2O_3 . *Naturwissenschaften* **1968**, *55*, 83.
- (35) Kim, S. W.; Iwamoto, S.; Inoue, M. Solvothermal Oxidation of Gallium Metal. *Ceram. Int.* **2009**, *35*, 1603–1609.
- (36) Li, L. D.; Wei, W.; Behrens, M. Synthesis and Characterization of α -, β -, and γ - Ga_2O_3 Prepared from Aqueous Solutions by Controlled Precipitation. *Solid State Sci.* **2012**, *14*, 971–981.
- (37) Smrčok, L.; Langer, V.; Krestan, J. γ -Alumina: A Single-Crystal X-ray Diffraction Study. *Acta Crystallogr., Sect. C: Cryst. Struct. Commun.* **2006**, *62*, i83–i84.
- (38) Marezio, M.; Remeika, J. P. Bond Lengths in the α - Ga_2O_3 Structure and the High-Pressure Phase of $\text{Ga}_{2-x}\text{Fe}_x\text{O}_3$. *J. Chem. Phys.* **1967**, *46*, 1862–1865.
- (39) Geller, S. Crystal Structure of β - Ga_2O_3 . *J. Chem. Phys.* **1960**, *33*, 676–684.
- (40) Lavalle, J. C.; Daturi, M.; Montouillout, V.; Clet, G.; Areán, C. O.; Delgado, M. R.; Sahibed-dine, A. Unexpected Similarities between the Surface Chemistry of Cubic and Hexagonal Gallia Polymorphs. *Phys. Chem. Chem. Phys.* **2003**, *5*, 1301–1305.
- (41) Williams, W. G.; Ibbserson, R. M.; Day, P.; Enderby, J. E. GEM — General Materials Diffractometer at ISIS. *Phys. B (Amsterdam, Neth.)* **1997**, *241*–243, 234–236.
- (42) Hannon, A. C. Results on Disordered Materials from the GEneral Materials Diffractometer, GEM, at ISIS. *Nucl. Instrum. Meth. Phys. Res., Sect. A* **2005**, *551*, 88–107.
- (43) Larson, A. C.; Von Dreele, R. B. *General Structure Analysis System*; Report LAUR 86-748; Los Alamos National Laboratory: Los Alamos, NM, 1994.
- (44) Toby, B. H. EXPGUI, a Graphical User Interface for GSAS. *J. Appl. Crystallogr.* **2001**, *34*, 210–213.
- (45) Soper, A. K. *GudrunN and GudrunX: Programs for Correcting Raw Neutron and X-Ray Diffraction Data to Differential Scattering Cross Section*; Technical Report RAL-TR-2011-013; Rutherford Appleton Laboratory, 2011.
- (46) Hannon, A. C.; Howells, W. S.; Soper, A. K. ATLAS: A Suite of Programs for the Analysis of Time-of-Flight Neutron Diffraction Data from Liquid and Amorphous Samples. *Inst. Phys. Conf. Ser.* **1990**, *107*, 193–211.
- (47) Lorch, E. Neutron Diffraction by Germania, Silica and Radiation-Damaged Silica Glasses. *J. Phys. C: Solid State Phys.* **1969**, *2*, 229–237.
- (48) Tucker, M. G.; Keen, D. A.; Dove, M. T.; Goodwin, A. L.; Hui, Q. RMCPProfile: Reverse Monte Carlo for Polycrystalline Materials. *J. Phys.: Condens. Matter* **2007**, *19*, 33521.
- (49) O'Dell, L. A.; Savin, S. L. P.; Chadwick, A. V.; Smith, M. E. Multinuclear MAS NMR Investigation of Sol-Gel and Ball-Milled Nanocrystalline Ga_2O_3 . *Appl. Magn. Reson.* **2007**, *32*, 527–546.
- (50) Delgado, M. R.; Morterra, C.; Cerrato, G.; Magnacca, G.; Areán, C. O. Surface Characterization of γ - Ga_2O_3 : A Microcalorimetric and IR Spectroscopic Study of CO Adsorption. *Langmuir* **2002**, *18*, 10255–10260.

- (51) Delgado, M. R.; Areán, C. O. Infrared Spectroscopic Studies on the Surface Chemistry of High-Surface-Area Gallia Polymorphs. *Z. Anorg. Allg. Chem.* **2005**, *631*, 2115–2120.
- (52) Vimont, A.; Lavalley, J. C.; Sahibed-Dine, A.; Areán, C. O.; Delgado, M. R.; Daturi, M. Infrared Spectroscopic Study on the Surface Properties of γ -Gallium Oxide as Compared to Those of γ -Alumina. *J. Phys. Chem. B* **2005**, *109*, 9656–9664.
- (53) Areán, C. O.; Delgado, M. R.; Montouillout, V.; Massiot, D. Synthesis and Characterization of Spinel-Type Gallia-Alumina Solid Solutions. *Z. Anorg. Allg. Chem.* **2005**, *631*, 2121–2126.